

Axial Flux BLDC Motor Liquid Cooling System: Modelling and Experimental Analysis

Tarsisius Kristyadi*, Marsono, Sahril Sayuti

Mechanical Engineering, Institut Teknologi Nasional Bandung Indonesia

Received 30 Aug 2021

Accepted 15 Jun 2022

Abstract

The paper describes the effect of cooling media and temperature on 20 KW axial flux BLDC motor performance using numerical and experimental analysis. The motor is applied in electric car with initially as natural air cooling, and it is modified as liquid cooling. Numerical and experimental analysis shows that cooling temperature has significant effect on power and efficiency of motor. Lower cooling temperatures produce higher motor power and efficiency. Based on experimental investigation, maximum power of water cooled BLDC motor can generate power of 25 kW and 81.0 % efficiency, while air cooled motor produces lower power and efficiency of 19.1 kW and 65.0 % respectively. Comparative analysis of motor performance based on model and experiment were presented as well. Maximum motor power calculated by model is slightly higher than that measured by experiment. It can be explained that in modeling, the friction losses on the bearings are neglected, while in the experiment, the friction loss remains a variable that affects the motor power output.

© 2022 Jordan Journal of Mechanical and Industrial Engineering. All rights reserved

Keywords: BLDC, axial flux, cooling, liquid, power.

1. Introduction

The development of electric vehicles encourages researchers to make these vehicles more efficient. Some of the studies aimed to improve the transmission system [1] and the electric motor performance. Air cooled axial flux BLDC motor used to drive electric cars loses power after several minute running due to motor overheat. Overheat on the electric motor leads to harmful effects, such as degradation of the insulation coil, demagnetization, increase of heat loss, decrease in the efficiency of the motor and reduction of the life time of the electric motor [2]. The heat generated due to the current through the windings causes an increase of temperature in various parts of the electric machine [3]. The increase in temperature reduces the insulation resistance of the windings, generates thermal stress, and reduces efficiency [4], and further causes machine failure [5].

Figure 1 shows motor performance which is affected by temperature variations. To generate torque at which is 1.65 Nm, motor at temperature 125°C requires a larger electric current compared to the motor at temperature 25°C. Peak power motor temperature of 125°C has 1.65 Nm torque while peak power motor temperature of 25°C was at torque 2.88 Nm [6].

It is indicated that the increase in temperature of the motor can affect performance of the electric motors [7]. Overheat on the motor can be avoided by using liquid cooling instead of air cooling. Several methods to increase the cooling rate can be carried out such as the addition of

fans on the heat transfer surface [8] and particle modification [9]. While the discussion of the flow characteristics numerically has also been discussed by several researchers [10]. Several studies on cooling material and cooling methods in electric motors have also been discussed in some literature [11,12,13,14]. Combination of nano fluid as cooling media and spiral cooling channels were applied as motor cooling system can increase the heat transfer capability of the cooling system and to reduce operating temperature of the electric motor [11,13]. Another investigation to prevent temperature rise in electric motor was used in metal-based phase change materials [14]. To increase heat transfer in phase change material heat sink, insertion of metal foam was applied [15].

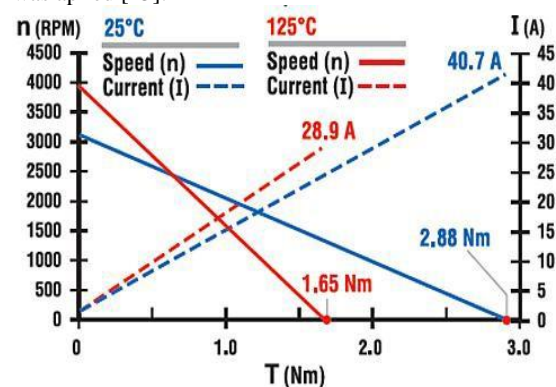


Figure 1. Comparison of BLDC motor performance with temperature variation [6]

* Corresponding author e-mail: kristyadi@itenas.ac.id.

For Cooling of existing motor installed on vehicle, simplified cooling modification is required. In this investigation, simplified flat waterjacket is applied in an axial flux BLDC motor. The goal of investigation is to determine the effectiveness of water cooling on axial flux BLDC motor numerically and experimentally.

2. Motor Description

The axial flux BLDC motor analyzed consists of the main components of the rotor, stator, bearings and casing. The motor stator consists of 2 stators where each stator consists of 12 identical cores. Armature core is made from pure iron powder with 99% Fe content mixed with carbon fiber resin as the bounding. This mixture of iron powder and resin consists of resin at 14% of the total weight of the mixture of iron powder and epoxy to form a carbon composite[16]. The stator winding (armature) uses copper wire coated with an insulator with a total diameter of 0.8 mm. The rotor on the BLDC motor consists of 8 pairs of permanent magnets. The magnets used in axial flux Brushless DC motors are neodymium types. Neodymium magnets (NdFeB, NIB or Neo magnet) are strong magnets that have a very wide range of applications [17,18,19,20]. This magnet is very popular for the use of electric machines based on permanent magnets. This magnetic strength can reach 440 kJ / m³, so it is suitable for use in BLDC motors [20].



Figure 2. Stator consists of core and armature

Figure 2. Shows the stator consisting of a core and copper windings forming a core and armature unit. There are 2 identical stators to form the BLDC that is analyzed. Figure 3 shows rotor piece which consists of 8 pairs of neodymium magnet. This rotor consists of 2 faces where each face is filled with 5 mm thick of magnets.



Figure 3. Magnetic rotor

General arrangement of the BLDC motor to be analyzed is described at Figure 4.

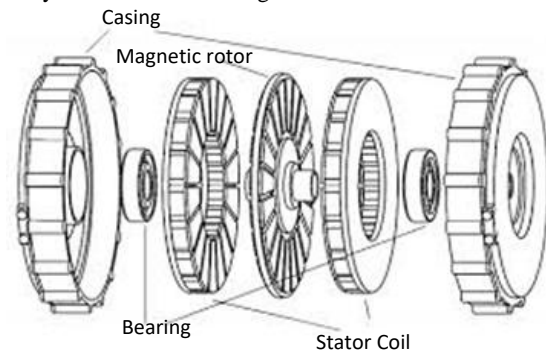


Figure 4. General arrangement of BLDC motor to be analyzed.

This motor has a nominal power of 20 kW and can produce a maximum power up to 30 kW.

Comparison between inner diameter of rotor and stator and the outer diameter is 0.58[19]. The motor has a maximum speed of 6000 rpm, powered by dc voltage of 72 v. For this analysis, the motor is initially air cooled and then liquid cooled.

3. Numerical Analysis

This paper discusses the modeling of 20 kW BLDC motor cooling process. The motor has rate power of 20 kW at voltage 72 V with 90% rate efficiency. The operation speed of the motor is about 2000-6000 rpm. Motor casing made by alluminum with dimension of 270 mm diameter and 306 mm height. In this simulation, electromagnetic losses such as core losses and copper losses are obtained by Maxwell equation, while losses due to bearing friction are neglected[16].

3.1. Model Description

Heat generation on BLDC Motor losses that occur in electric motors can be classified as follows:

3.1.1. Resistive Losses

Resistive losses are generally the main component of power losses in BLDC motors and are calculated as[22]:

$$P_r = m I_{ph}^2 R_{ph} \quad (1)$$

where I_{ph}^2 is the current phase, m is the number of phases and R_{ph} is the resistance which varies depend on temperature[22].

3.1.2. Loss per Unit Mass due to Hysteresis (Ph)

The core stator is made of insulated silicon steel lamination. Therefore, variations in magnetic flux due to magnetic rotation produce Eddy current losses and hysteresis losses in the laminate. This loss is estimated individually for the yoke tooth stator as different variations in the inside field. Loss of mass per unit due to hysteresis, Eddy current in yoke stator and Eddy current in tooth stator is calculated as [22,23]:

$$P_h = K_h f^\alpha B_m^\beta \quad (2)$$

Where B_m is the peak density of the flux f is the frequency of the flux variation, K_h, α, β is the fit curve calculated from the data of the loss of the laminate.

3.1.3. Eddy Current Losses on Stator Yoke (P_{ey})

To calculate Eddy current losses in the stator yoke, the following equation can be used [22,24]:

$$P_{ey} = K_e \frac{8 f^2 B_m^2}{\pi \beta_m} \quad (3)$$

Where B_m is the peak flux density, f is the frequency of the flux variation, β_m is the arc of the tooth and width of the mast respectively in the electric radians, K_e is the curve of the fit constant calculated from the data of the loss of the laminate.

3.1.4. Eddy Current Losses on Stator Tooth (P_{et})

To calculate eddy current losses in a tooth stator, the following equation can be used [24,25]:

$$P_{et} = K_e \frac{4 f^3 B_m^2}{\pi \alpha_{tt}} \left[2 - \frac{\pi - \beta_m}{\alpha_{tt}} \right] \quad (4)$$

where B_m is the peak flux density f is the frequency of the flux variation, α_{tt} and β_m is the arc of the tooth and the pile width respectively in the electric radians, K_h, K_e, α, β are the fit curve curves calculated from the data on the loss of the laminate [25].

3.1.5. Heat Transfer Model

The heat transfer modelling is illustrated in following figure.

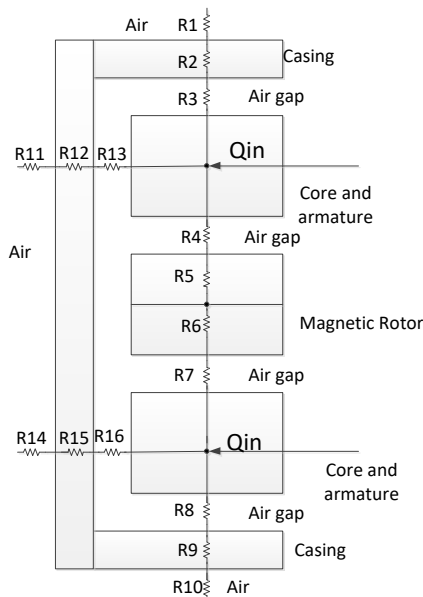


Figure 5. Thermal circuit model of air cooled motor

Figure 5 shows the thermal circuit of air cooled motor, where heat generated from core and armature is transferred to atmospheric air. Thermal circuit model of liquid cooled motor is shown in Figure 6. In this figure, heat transfer from core and armature is transferred to atmospheric air axially and also transferred to liquid cooler radially.

In this analysis, the heat transfer model is divided into 2 cases, namely the air cooled motor and the liquid cooled motor. In the first case, where the motor using air-cooling, axial heat transfer occurs from the core and armature to the outside air through the air gap by convection, to the casing

by conduction, then by convection and radiation from the casing surface to the air. Whereas heat transfer in the radial direction occurs from the core and armature through the air gap by convection, through casing by conduction and continues from the surface of the casing to the outside air by radiation.

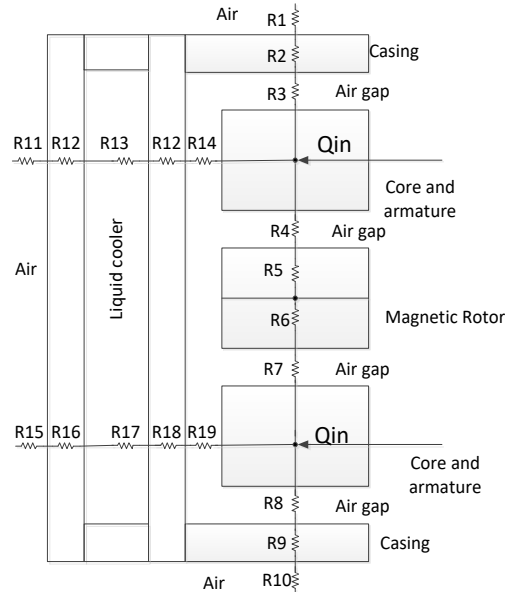


Figure 6. Thermal circuit model of liquid cooled motor

Model illustration of the first case is shown in Figure 5. In the second case as shown at Figure 6, the motor is cooled using liquid (water), the cooling process in the axial direction is the same as in the first case, while the cooling in the radial, there is an additional heat transfer mode. The additional mode occurs from inner surface of the casing to the outside air through convection in water and conduction from the inner surface to the outer surface of the casing.

Core and armature winding are heat sources on this motor that can be simplified as heat flux. In this model, air gap between the armature/core and casing, and air gap between core/armature and magnetic rotor use silicone thermal grease with a thermal conductivity of 6.2 W / mK as thick as 0.5 mm [26,27,28].

The magnitude of heat transfer Q from the core and winding armature to the atmospheric air depends on the convection coefficient and therefore, its estimation becomes the routine of thermal analysis. The heat transfer by convection is described by below equation [29]:

$$Q = hA(T_s - T_a) \quad (5)$$

Where A is surface area, T_a and T_s are atmospheric and surface temperature respectively and h is convection coefficient that described as [29]:

$$h = \frac{k}{D} (0.11) [0.5 Re^2 + Gr_r Pr]^{0.35} \quad (6)$$

where :

D is diameter

k is thermal conductivity

Re is Reynolds number

Gr is Grashof number

Pr is Prantl number

T_s is Temperature of surface (casing and core)

T_a is air or liquid temperature

3.1.6. Model of Mechanical Power of Rotor

Rotor rotation is governed by the mechanical equation below[30]:

$$J_m \frac{d\omega}{dt} = T_e - T_L + D\omega \tag{7}$$

where J_m is the total moment of inertia, ω is the rotor speed; T_e is the electromagnetic torque, D is the damping coefficient and T_L is the torque required to drive the load.

Rotor inertia is based on the assumption that all parts of the rotor rotate around the center of the shaft [30]:

$$J_{shaft} = 2\pi\rho L_{shaft} \left(\frac{D_{shaft}}{2}\right)^4 \tag{8}$$

3.1.7. Electrical-Mechanical Relation Model

Relation between electrical power and mechanical power is described using following equation [30,31]:

$$P_{elect} = P_{mech\ shaft} + P_r + P_h + P_{ey} + P_{et} + P_{thermal\ loss} + P_f \tag{9}$$

where $P_{mech\ shaft}$ is mechanical power by motor shaft, P_f is bearing friction losses which is neglected. From above equation, for numerical (modelling) analysis mechanical power generated by motor shaft is described as[30,32]:

$$P_{mech\ shaft} = P_{elect} - P_r - P_h - P_{ey} - P_{et} - P_{thermal\ loss} \tag{10}$$

In this case[31]:

$$P_{elect} = V.I \tag{11}$$

Where I is electrical current and V is voltage.

3.2. Calculation Procedure

The purpose of the simulation is to calculate the power and efficiency of the motor. Electrical energy is supplied to the motor with voltage and current parameters of 72 V and 400 A respectively. The input energy is transferred to mechanical energy (P_{mech}) and losses, which consists of resistive losses (P_r), hysteresis (P_h), Eddy current on stator yoke (P_{ey}), Eddy current on stator tooth (P_{et}) and heat transfer loss. The boundary condition can be described as follows[34,35]:

Table 1. Boundary condition of motor model

Specify Boundary Name	Type	Specify Continuum Name	Type
Inlet	Velocity Inlet	External_Fluid	Fluid
Outlet	Pressure Out	Internal_Fluid	Fluid
Wall_Surrounding	Wall	Heatsink	Solid
Wall_Heatsink	Wall	Rotor	Solid
Wall_Rotor	Wall	Winding	Solid
Wall_Winding	Wall	Core	Solid
Wall_Core	Wall		

Actual heat transfer will occur in 3D in all directions following the temperature differences that occur. The heat source on the axial flux BLDC motor is on the winding and core where heat flux (Q_{in} at upper stator and Q_{in} at lower stator) are transferred axially and radially. At upper side, heat flux transmitted in axial direction will be through convection with thermal resistance of R_3 , conduction on casing with thermal resistance of R_2

followed by radiation from casing surface to atmospheric air. In the other hand, the heat flux is transfer axially to rotor magnet by convection and conduction with thermal resistance R_4 and R_5 respectively. Radial heat transfer occur when heat generated by stator is transferred to surrounding air by convection (R_{13}), then conduction (R_{12}) and followed by radiation with thermal resistance R_{11} . Likewise at lower side, heat flux is transferred in axial direction by convection with thermal resistance R_8 , conduction on casing with thermal resistance R_9 followed by radiation from casing surface to atmospheric air with thermal resistance R_{11} . The heat flux is also transferred axially to rotor magnet by convection with thermal resistance of R_7 and conduction with thermal resistance R_6 . Similar to upper side, radial heat transfer at lower side occurs when heat generated by stator is transferred to surrounding air by convection (R_{16}), then conduction (R_{15}) and followed by radiation with thermal resistance R_{14} .

Above description is the modeling of heat transfer in an air-cooled motor. While the calculation of heat transfer radially in a liquid-cooled motor, there is an additional mode, namely convection in the radial direction from the casing to the liquid cooler. Referring to the figure, convection occurs from the surface of the casing to the coolant which is symbolized by R_{13} on the upper side and R_{17} on the lower side. R_{12} and R_{16} show the conduction heat transfer resistance in the casing while R_{11} and R_{15} are radiation thermal resistance from the casing surface to atmospheric air.

3.3. Calculation Result

The first modeling is a 20 KW BLDC motor given an electrical energy and cooling by atmospheric air with temperature of 27 °C. Motor rotation at maximum speed at 6000 rpm. The analysis is focused on the thermal conditions between the stator core and the rotor, which became a heat source and requires cooling. While other losses are considered constant depending on the properties of the magnetic material, of core and coil. Figure 7 describes the temperature distribution between the stator armature, casing and magnetic rotor on the upper side of the motor axially. It is assumed that the motor is upper and lower symmetric, hence the characteristic of lower side is similar with the upper side.

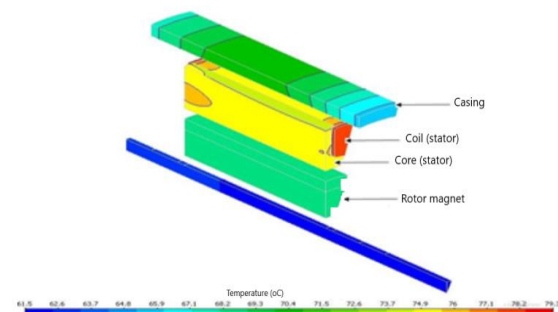


Figure 7. Temperature distribution of inner motor based on air cooled

It can be seen that maximum temperature occurs at armature especially at coil. Temperature difference between maximum and lowest temperature is about 13°C. And temperature difference between casing surface at axial

position is about 42°C. At radial heat transfer condition, temperature distribution of the BLDC motor can be seen at the following figure. In Figure 8 below, it can be seen that core and armature temperature are relatively uniform.

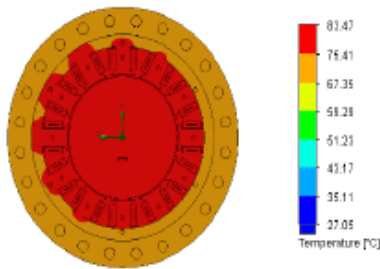


Figure 8. Motor temperature distribution at radial direction with air cooled

The casing temperature in the radial direction is also relatively hot, and the difference between the casing temperature and the air temperature is also relatively the same, which is around 42 °C. Figure 9 shows the temperature distribution in the radial direction (seen in cross section). Prediction of temperature distribution along motor casing contain fin is similar with other calculation [36].

The second modeling is a water cooled 20 kW BLDC. In this case, the motor is modified by providing a water jacket and wrapped with a second casing for the cooler. Temperature of water as liquid cooler is set as 20°C. In this condition, thermal conductivity of water is 12 W/mK [29].

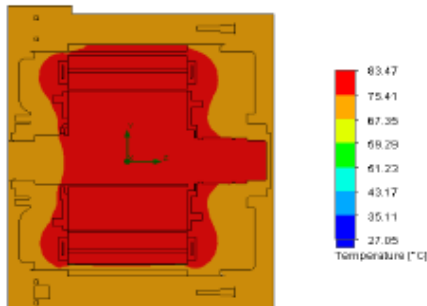


Figure 9. Cross section temperature distribution on air cooled BLDC motor

Similar with first model, temperature distribution of stator, rotor magnet and casing axially is analyzed. Figure 10 show the temperature distribution of above referred. The maximum temperature is lower than air cooling motor. Temperature difference between casing surface at axial position is about 28°C.

Temperature distribution analysis at radial direction is shown at the Figure 11. It can be seen that maximum motor temperature is relatively lower than air cooled motor. More clearly, the temperature difference between the casing surface and the water cooler is shown in the Figure 12. From the figure, the difference between the casing and the coolant reaches 47°C.

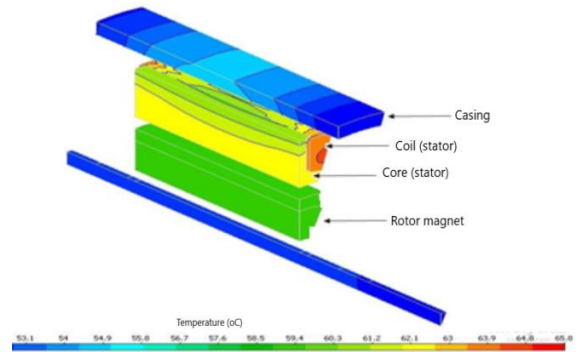


Figure 10. Temperature distribution of inner motor based on water cooled

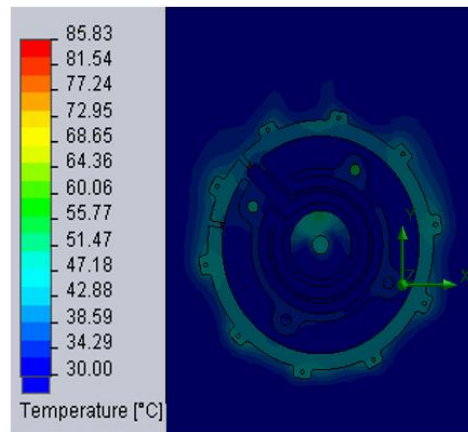


Figure 11. Water cooled Motor temperature distribution at radial direction

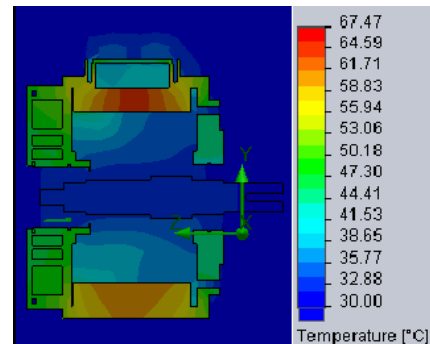


Figure 12. Cross section temperature distribution on water cooled BLDC motor

Similar calculation using various water temperature, air temperature and motor speed. Water temperature is set as 20°C, 22°C, 24°C, 50°C, 60 °C and 70°C. Ambient air temperature is varied from 27°C to 50°C. And motor speed is varied form 1500 rpm to 6000 rpm

3.3.1. Motor Power and efficiency Calculation

By using numerical analysis, based on previous calculation procedure, motor power and efficiency can be defined and summarized in the following table:

Table 2. Motor power and efficiency calculation result based on air cooled motor modelling

Air temperature (°C)	Motor speed (rpm)	Motor power (kW)	Motor efficiency
27	6000	22500	0.781
27	3000	21900	0.760
30	6000	21800	0.757
30	3000	21250	0.738
40	6000	19100	0.663
40	3000	18650	0.648
50	6000	16780	0.583
50	3000	15800	0.549

Table 3. Motor power and efficiency calculation result based on water cooled motor modelling

Water temperature (oC)	Motor speed (rpm)	Motor power (kW)	Motor efficiency
20	6000	25400	0.882
20	3000	25150	0.873
22	6000	24700	0.858
22	3000	24300	0.844
24	6000	23600	0.819
24	3000	23050	0.800
50	6000	17020	0.591
50	3000	16550	0.575
60	6000	14250	0.495
60	3000	13800	0.479
70	6000	13100	0.455
70	3000	12060	0.419

From above table, it can be seen that cooler temperature have significant effect for maximum motor power and efficiency, while motor speed give small effect.

4. Experimental Analysis

The air cooling and liquid cooling BLDC motor was tested using dynamometer test bed. The dynamometer is equipped with electronic speed sensor, power sensor, temperature sensor based on Arduino. The test bed is illustrated at Figure 13.

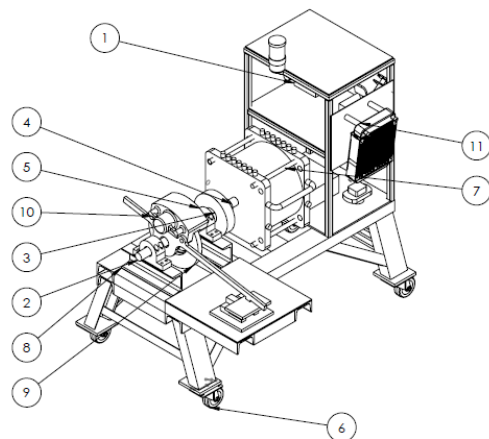


Figure 13. Motor test bed

Where:

1. Load controller
2. Speed sensor
3. 1st Coupling
4. 2nd coupling

5. Pillow block
6. Caster wheel
7. Motor
8. Bearing support
9. Temperature sensor
10. Power meter
11. Panel for instrument

The experimental analysis investigates the effect of air cooling and liquid cooling temperature on BLDC motor power. Motor speed was variated by load variation by dynamometer control. Voltage and current were set of 72 V and 400 A respectively. In first experiment, the BLDC motor was cooled by 25°C atmospheric air. The cooling temperature was set as fix. In liquid cooling case, motor was cooled by water with various temperature from 20°C to 70°C. Electrical power input was similar with air cooled case. The result of experiment is described in the following figure. In Figure 14, effect of cooling temperature on motor power is described. This figure shows that higher cooler temperature cause lower power. This is in line with the theory described in the introduction, that the higher the temperature is, the lower the magnetic strength gets, causing the motor power to decrease as well. Cooling media also has effect on motor power. Liquid cooler has higher heat transfer rate than air cooler. Higher thermal conductivity of water provides a greater cooling rate so that the stator and rotor temperatures are relatively low, resulting in higher motor power. This is shown in Figure 15. As power increases, the water cooled motor efficiency is also higher than air-cooled motors. This can be seen in the Figure 16. From Figure 15 and Figure 16, it can be seen that liquid cooling motor can produce maximum power of 25 kW and 81.0 % of efficiency, while air cooling motor can produce maximum power of 19.1 kW and 65.0% efficiency

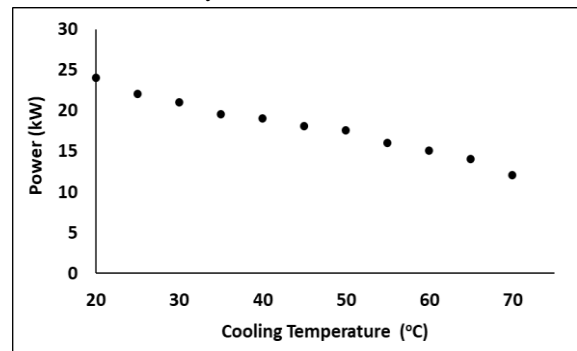


Figure 14. Effect of cooling temperature to motor power.

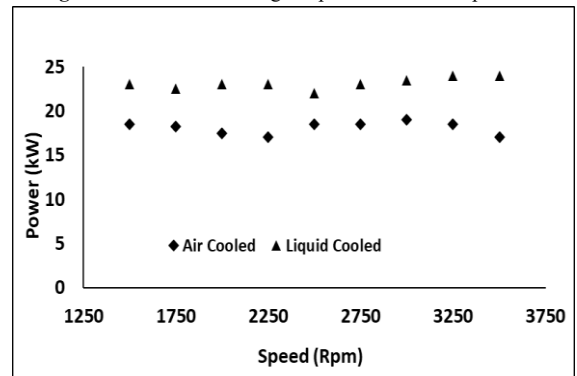


Figure 15. Motor power based on cooler type at various speed.

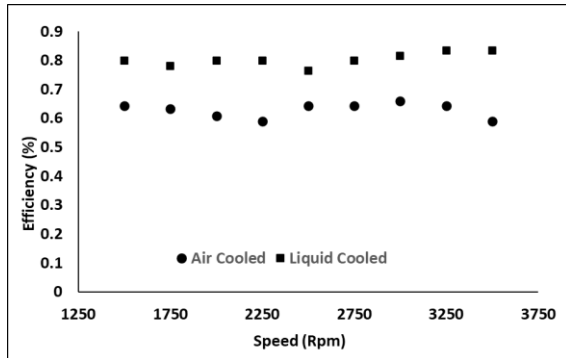


Figure 16. Motor power based on cooler type at various speed.

The final investigation is a comparative analysis of motor performance based on model and experiment. From Figure 17, it can be seen that maximum motor power calculated by model is slightly higher than that measured by experiment. It can be explained that in modeling, the friction losses on the bearings are neglected, while in the experiment, the friction loss remains a variable that affects the motor power output.

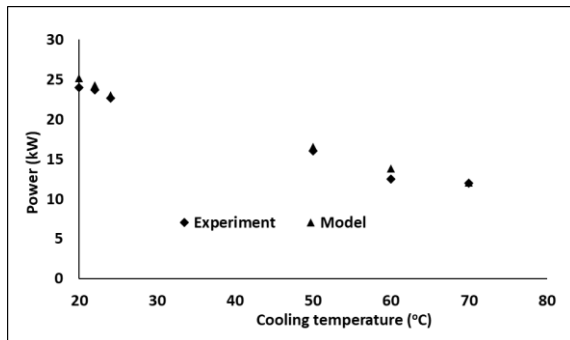


Figure 17. Comparative of motor power based on model and experiment.

5. Conclusion

Effect of cooling temperature and cooling media on axial flux BLDC motor power and efficiency were presented. 20 kW of BLDC motor performance with air cooling and water cooling was investigated numerically and experimentally. From numerical analysis, the motor power was calculated based on input power minus losses power and efficiency was calculated based power input and power output. The calculated power was compared with measured power that was conducted on motor test bed. The Numerical and experimental method shows that cooling temperature has significant effect on power and efficiency of motor. Lower of cooling temperature produces higher motor power and efficiency. Based on experimental investigation, at normal condition, maximum power of water cooled BLDC motor can generate power of 25 kW and 81.0 % efficiency, while air cooled motor produces lower power and efficiency of 19.1 kW and 65.0 % respectively. Comparative analysis of motor performance based on model and experiment was presented as well. Maximum motor power calculated by model is slightly higher than that measured by experiment. It can be explained that in modeling, the friction losses on the bearings are neglected, while in the experiment, the

friction loss remains a variable that affects the motor power output

Acknowledgment

This research paper is funded from Indonesia Government in "Penelitian Terapan Unggulan Perguruan Tinggi" scheme year 2019.

References

- [1] Qingyong Z., Wanga Y., Lina W., Luo Y., Wua X., "Contact mechanics analysis and optimization of shape modification of electric vehicle gearbox". Jordan Journal of Mechanical and Industrial Engineering, Volume 14, Number 1, March. 2020 . P 15 – 24.
- [2] Vu, Duc Thuan, "New cooling system design of bldc motor for electric vehicle using computation fluid dynamics modeling". Journal of the KSTLE Vol. 29, No. 5, October 2013, pp. 318~323.
- [3] Fasil, Muhammed, "Numerical and experimental investigation of heat flow in permanent magnet brushless dc hub motor". SAE International J. Alt. Power./ Volume 4, Issue 1 (May 2015).
- [4] Cezario, Cassiano A., "Transient thermal analysis of an induction electric motor". 18th International Congress of Mechanical Engineering November 6-11, 2005, Ouro Preto, MG
- [5] Kuria, James dan Hwang, Pyung. Optimizing heat sink geometry for electric vehicle bldc motor using CFD. Kenyatta University of Agriculture and Technology, Kenya, 2017
- [6] Chandrakant, Shinde S., "Numerical and experimental analysis of heat transfer through various types of fin profiles by forced convection". International Journal of Engineering Research & Technology (IJERT) ISSN: 2278-0181 Vol. 2 Issue 7, July –2013
- [7] Faiz, J., Ganji, B., Carstensen, C.E., "Temperature rise analysis of switched reluctance motors due to electromagnetic losses". IEEE Trans. Magn., 2009, 45, (7), pp. 2927–2934
- [8] Samadifar M and Toghraie D., "Numerical simulation of heat transfer enhancement in a plate-fin heat exchanger using a new type of vortex generators". Applied Thermal Engineering vol.133, March 2018, pp.671-681.
- [9] Toghraie D., Afrand M., Zadeh A.R., Akbari H.A., "Numerical investigation on the flow and heat transfer of a multi-lobe particle and equivalent spherical particles in a packed bed with considering the wall effect". International Journal of Mechanical Sciences, Vol 138-139 April 2018 pp.350-367.
- [10] Toghraie D., Moraveji A., "Computational fluid dynamics simulation of heat transfer and fluid flow characteristics in a vortex tube by considering the various parameters". International Journal of Heat and Mass Transfer Vol. 113, Oct. 2017, pp. 432-443
- [11] Deriszadeh A, de Monte F. "On Heat Transfer Performance of Cooling Systems Using Nanofluid for Electric Motor Applications". Entropy. 2020; 22(1):99. <https://doi.org/10.3390/e22010099>
- [12] Deriszadeh, F. de Monte, M. Villani and L. Di Leonardo, "Hydrothermal performance of ethylene glycol and water mixture in a spiral channel for electric motor cooling," 21st European Conference on Power Electronics and Applications (EPE '19 ECCE Europe), 2019, pp. 1-10, doi: 10.23919/EPE.2019.8914967.
- [13] Deriszadeh A, de Monte F., "Performance evaluation of the electric machine cooling system employing nanofluid as an

- advanced coolant". *ChemEngineering*. 2021;5(3):53. <https://doi.org/10.3390/chemengineering5030053>
- [14] Deriszadeh, A, de Monte, F, & Villani, M., "Numerical thermal performance investigation of an electric motor passive cooling system employing phase change materials". *Proceedings of the ASME 2021 Heat Transfer Summer Conference collocated with the ASME 2021 15th International Conference on Energy Sustainability*. ASME 2021 Heat Transfer Summer Conference. Virtual, Online. June 16–18, 2021. V001T08A006. ASME. <https://doi.org/10.1115/HT2021-63506>
- [15] Ahmad K. A.M, Jawarneh A.M, Ababneh A.K., Dalgamoni H.N., "Numerical investigation of the cooling performance of pcm-based heat sinks integrated with metal foam insertion". *Jordan Journal of Mechanical and Industrial Engineering*, Volume 15, Number 2, June. 2021. P 191 – 197.
- [16] Fu, L. M., Lin, C., Chang, C. L., Chang, J., & Tsai, C. H., "Numerical investigation into thermal behavior of brushless permanent magnet motors". *Advanced Materials Research*, 199–200, 1518–1522.
- [17] Han, S., Jahns, T.M., Zhu, Z.Q., "Analysis of rotor core eddy-current losses in interior permanent magnet synchronous machines". *Industry Applications Society Annual Meeting*, Edmonton, Alta, October 2008
- [18] NEOREC series neodymium iron boron magnet datasheet'. TDK Corporation, May 2011. Available at: <http://tdk.co.jp/>
- [19] Constantinides, S., The demand for rare earth materials in permanent magnets. *Arnold Magnetic Technologies*. Available at: <http://arnoldmagnetics.com/>, [Accessed 18 July 2019]
- [20] Trout, S.R., "Material selection of permanent magnets, considering the thermal properties correctly". *Proc. The electric manufacturing and coilwinding conf.*, Cincinnati, OH, October 2001.
- [21] Gieras, Jacek F., Wang, Rong-Jie, Kamper, Maarten J. *Axial flux permanent magnet brushless machines book*. Springer; 2008.
- [22] Zhang, Y., Cheng, M.C., Pillay, P., "Magnetic characteristics and excess eddy current losses". *Industry Applications Society Annual Meeting*, Houston, TX, 2009
- [23] Nalakath, S., Preindl, M., Yang, Y., "Modeling and analysis of core losses of an IPM magnet machine for online estimation purposes". *Annual Conf. of IEEE Industrial Electronics Society*, Yokohama, Japan, 2015
- [24] Mthombeni, T.L., Pillay, P., "Physical basis for the variation of lamination core loss coefficients as a function of frequency and flux density". *Annual Conf. on IEEE Industrial Electronics*, Paris, November 2006
- [25] Takahashi, N., Morishita, M., Miyagi, D., "Examination of magnetic properties of magnetic materials at high temperature using a ring specimen". *IEEE Trans. Magn.*, 2010, **46**, (2), pp. 548–551
- [26] Selection of electrical steels for magnetic cores. AK Steel. Available at: <http://aksteel.com/>, [Accessed 16 July 2019]
- [27] Standard classification of insulating coatings for electrical steels by composition, relative insulating ability and application. *American Society of Testing and Materials*, ASTM A 976-13, 2015
- [28] DuPONT NOMEX Paper Type 410. DuPONT. Available at: <http://www.dupont.com>, [Accessed April 2020]
- [29] Chang, C.C., Cheng, C.H., Ke, M.T., "Experimental and numerical investigations of air cooling for a large-scale motor". *Int. J. Rotating Mach*, 2009, pp. 1–7
- [30] Yang, Y., Arshad-Ali, K., Roeleveld, J., "State-of-the-art electrified powertrains: hybrid, plug-in hybrid, and electric vehicles". *Int. J. Powertrains*, 2016, **5**, (1), pp. 1–28
- [31] Yang, Y., Schofield, N., Emadi, A., "Integrated electro-mechanical doublerotor compound hybrid transmissions for hybrid electric vehicles". *IEEE Trans. Veh. Techno.*, 2016, **65**, (6), pp. 4687–4699
- [32] Bilgin, B., Magne, P., Malysz, P., "Making the case for electrified transportation". *IEEE Trans. Transp. Electrification*, 2015, **1**, (1), pp. 4–17
- [33] Gerada, D., Mebarki, A., Brown, N.L., "High-speed electrical machines: technologies, trends, and developments". *IEEE Trans. Ind. Electron.*, 2014, **61**, (6), pp. 2946–2959
- [34] Zhang, Y., Ruan, J., Huang, T., "Calculation of temperature rise in aircooled induction motors through 3-D coupled electromagnetic fluid dynamic and thermal finite-element analysis". *IEEE Trans. Magn.*, 2012, **48**, (2), pp. 1047–1050
- [35] Yoheswaran, B., Pullen, K.R., "Flow and convective heat transfer in disk-type electric machines with coolant flow". *Int. Conf. on Electrical Machines (ICEM)*, 2014
- [36] Mohammad S., "Computational fluid dynamics simulation of plate fin and circular pin fin heat sinks". *Jordan Journal of Mechanical and Industrial Engineering*, Volume 10, Number 2, June. 2016. P 99 – 104.